THE JOURNAL OF PHYSICAL CHEMISTRY B

Article

pubs.acs.org/JPCB

Experimental and Computational Evidence of Metal-O_2 Activation and Rate-Limiting Proton-Coupled Electron Transfer in a Copper Amine Oxidase

Yi Liu,[†] Arnab Mukherjee,[†] Nadav Nahumi,[†] Mehmet Ozbil,[§] Doreen Brown,[‡] Alfredo M. Angeles-Boza,[†,∥] David M. Dooley,*[,‡,⊥] Rajeev Prabhakar,*[,§] and Justine P. Roth*[,†]

[†]Department of Chemistry, Johns Hopkins University, 3400 North Charles Street, Baltimore, Maryland 21218, United States

[‡]Department of Chemistry and Biochemistry, Montana State University, Bozeman, Montana 59717, United States

[§]Department of Chemistry, University of Miami, 1301 Memorial Drive, Coral Gables, Florida 33146, United States

Supporting Information

ABSTRACT: The mechanism of O_2 reduction by copper amine oxidase from *Arthrobacter globiformus* (AGAO) is analyzed in relation to the cobalt-substituted protein. The enzyme utilizes a tyrosine-derived topaquinone cofactor to oxidize primary amines and reduce O_2 to H_2O_2. Steady-state kinetics indicate that amine-reduced CuAGAO is reoxidized by O_2 >10^3 times faster than the CoAGAO analogue. Complementary spectroscopic studies reveal that the difference in the second order rate constant, $k_{cat}/K_M(O_2)$, arises from the more negative redox potential of $Co^{III/II}$ in relation to $Cu^{II/I}$. Indistinguishable competitive oxygen-18 kinetic isotope effects are observed for the two enzymes and modeled computationally using a calibrated density functional theory method. The results are consistent with a mechanism where an end-on (η^1)-metal bound superoxide is reduced to an η^1-hydroperoxide in the rate-limiting step.

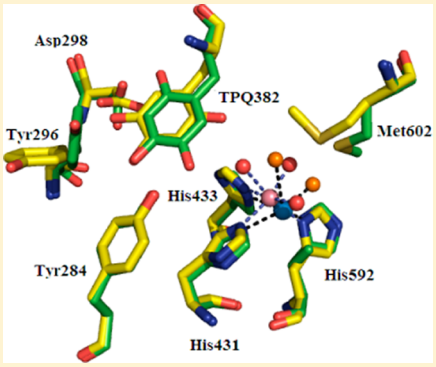

INTRODUCTION

The utilization of O_2 as an oxidant in "bio-inspired" chemical synthesis[1−5] has ignited significant interest in metalloprotein oxidases.[6−10] Although computational studies have become increasingly common,[11−16] the experimentation needed to test calculated pathways remains limited. In the case of copper amine oxidases, O_2 reduction to H_2O_2 is physiologically significant,[17] serving diverse functions in amine metabolism/catabolism, vascular adhesion proteins, and the inflammatory response.[18,19] Yet the roles of the redox-active metal and the surrounding protein environment have not been understood.

The copper amine oxidase from *Arthrobacter globiformus* (AGAO) is an extremely well-studied protein.[20−22] It has been shown to possess ∼0.7 Cu^{II} and 2,4,5-trihydroxyphenylalanine quinone (TPQ) cofactor, derived from post-translational oxidation of a specific tyrosine,[23,24] per monomeric subunit. The enzyme uses TPQ to mediate primary amine oxidation and reduction of O_2 to H_2O_2, while forming NH_3 as a byproduct, in eqs 1 and 2 below.

$$E_{ox} + RCH_2NH_3^+ \rightarrow E_{red} + RCH_2O \quad (1)$$

$$E_{red} + O_2 + H_2O \rightarrow E_{ox} + H_2O_2 + NH_3 \quad (2)$$

The apoprotein of AGAO is readily prepared and reconstituted with cobaltous ion, for the purpose of testing the role of the metal ion during the oxidative phase of catalysis.[25−31] Here it is demonstrated for the first time that Co^{II}-reconstituted AGAO undergoes rapid oxidation to Co^{III} upon exposure to the H_2O_2 product of enzyme turnover. Previous works have neglected this reaction and assumed that neither Co^{II} nor Cu^{II} undergoes a change in redox state during enzyme catalysis.[32]

The E_{red} in eq 2 may involve complex internal redox chemistry in certain copper amine oxidases,[33−36] where the active site metal and primary amine-reduced cofactor, referred to throughout as TPQ_{red}, undergo a rapid and reversible electron transfer that interconverts the Cu^{II} TPQ_{red} and Cu^{I} $TPQ_{sq•+}$ (eq 3). The same equilibrium is likely established but harder to detect in CoAGAO because of the more negative redox potential of $Co^{III/II}$ relative to $Cu^{II/I}$.

The protonation state of the semiquinone is uncertain, yet the absence of spectral changes under acidic and basic conditions suggests reactivity via a single species with a delocalized charge. Such charge delocalization is supported by extensive hydrogen bonding within the active site.[20] For the purposes of this study, the O_2-reactive form of the wild-type enzyme is referred to as Cu^{I} $TPQ_{sq•+}$ with the implicit assumption that the proton may resides on a ring substituent or a nearby base. Results described below suggest the same is true for the cobalt-containing AGAO, wherein Co^{III} TPQ_{red} is present in an unfavorable equilibrium with the Co^{II} $TPQ_{sq•+}$

Received: December 10, 2012
Revised: December 13, 2012

   dx.doi.org/10.1021/jp3121484 | *J. Phys. Chem. B* XXXX, XXX, XXX−XXX

Table 1. Acquisition Parameters Used to Collect X-Band EPR Spectra at 9.47 Ghz

protein	temperature (K)	attenuation (dB)	modulation amplitude (G)	modulation frequency (Khz)	receiver gain
CuAGAO	77	15	1	100	5.02×10^4
	295	10	20	100	5.02×10^3
CoAGAO	4	20	32	100	5.02×10^3
	18	20	32[a] or 10[b]	100	5.02×10^5
	91	40	10	100	5.02×10^3

[a]Used in experiments with H_2O_2. [b]Used in experiments with excess PEA and O_2.

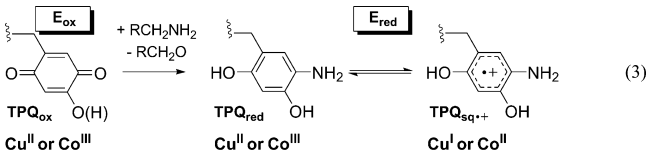

(3)

Kinetic and spectroscopic analyses are applied here, together with oxygen-18 isotope effects and complementary density functional theory (DFT) calculations, to provide a virtual roadmap to dissecting mechanisms of transition-metal mediated O_2 activation which occur during enzyme catalysis. Although it is generally difficult to identify rate-limiting steps in such oxidative transformations, oxygen isotope fractionation from natural abundance levels provides a potential solution.

Competitive oxygen-18 kinetic isotope effects (^{18}O KIEs) have been determined on a number of stoichiometric and catalytic reactions.[36−47] These probes are particularly useful when combined with DFT calculations, which can provide information regarding transition states that would not otherwise be accessible.[11,48−55] The ^{18}O KIE is defined by the ratio of rate constants, $k_{cat}/K_M(^{16,16}O_2)$ to $k_{cat}/K_M(^{16,18}O_2)$. Therefore, it reflects bonding changes that occur in steps beginning with O_2 encounter and the enzyme leading up to and including the first irreversible step. The DFT method used to compute ^{18}O KIEs has been calibrated using oxygen-18 equilibrium isotope effects (^{18}O EIEs) on a number of reversible O_2 activation reactions,[56,57] specifically those which involve the formally assigned $Cu^{II}(O_2^{-1})$ and $Co^{III}(O_2^{-1})$ complexes. Thus, this computational approach should be ideal for addressing reactions of copper amine oxidases and the cobalt-substituted variants, which exhibit diminished O_2 reactivity.

Though ^{18}O KIEs have now been measured on a number of enzymatic[38−47] and nonenzymatic[11,36] reactions of O_2, DFT has only recently been applied to predict the isotope effects.[49,58,59] The agreement between experiment and theory serves as a fairly rigorous criterion for evaluating transition states. The Transition State Theory formalism in eq 4 requires isotopic imaginary modes to define the isotope effect on the reaction coordinate ($^{18}\nu_{RC}$) and 3*N*-6 stable isotopic vibrations to define the isotope effect on the pseudoequilibrium constant for attaining the transition state ($^{18}K_{TS}$) relative to the separated reactants composed of *N* atoms. The expression is solved for the relevant O_2 isotopologues at natural abundance levels, i.e., $^{16,16}O_2$ and $^{16,18}O_2$, using the transition state identified by DFT calculations. The Cu^{II} and Co^{III} end-on superoxide (η^1-O_2^{-1}) precursors serve as starting points, with the surrounding active site modeled based on crystal structures of copper and cobalt-containing AGAO.[20]

$$^{18}\text{O KIE} = {}^{18}\nu_{RC} \times {}^{18}K_{TS} \quad (4)$$

EXPERIMENTAL SECTION

CuAGAO was expressed recombinantly[21] and CoAGAO was prepared from the apoprotein following an optimized protocol.[25] Chemicals were obtained from commercial sources in the highest grade available. Specifically deuterated *β*-phenethylamine (PEA) and benzylamine (BA) were supplied by C/D/N isotopes. D_2O was supplied by Cambridge Isotopes Laboratories and H_2O with 18 megaΩ resistivity was obtained from a Millipore ultrafiltration unit. An Omega PHB-213 meter was used to determine the pH. The relation: pD = $pH_{reading}$ + 0.4 was assumed. Sodium phosphate or potassium phosphate was used to control the solution pH or pD. Relative buffer concentrations were manipulated to maintain constant ionic strength without introducing additional salts. All measurements were conducted at pH 7.2, μ = 0.1 M and 22 ± 0.2 °C unless noted.

Electronic absorption spectra were recorded on an Agilent 8453 diode array spectrometer. Samples were initially prepared under rigorously anaerobic conditions in a N_2-filled glovebox (MBraun). In a typical experiment, CuAGAO or CoAGAO (30−50 μM) was reacted with 4−5 equivalents of PEA and 20 equivalents of H_2O_2 (ε_{240} = 43.6 M^{-1} cm^{-1}) in either order. Relatively high protein concentrations were used to ensure that ≥10% yield of the $TPQ_{sq\bullet+}$ would be detectable, based on the reported extinction coefficient $\varepsilon_{468\ nm}$ = 4500 M^{-1} cm^{-1}.[33]

Characterization by X-band electron paramagnetic resonance (EPR) spectroscopy was performed on the Co^{II}-reconstituted AGAO initially at Montana State University using a Bruker 9.79 Ghz spectrometer.[60] All other EPR spectra, presented in this work, were collected at Johns Hopkins University on an Bruker spectrometer operating at 9.47 Ghz. Acquisition parameters were optimized based on power saturation experiments and tabulated. In certain instances, temperatures were varied to expose the high-spin Co^{II} species[61−63] and the distinctive hyperfine coupling of the $TPQ_{sq\bullet+}$.[33−35] Signals were analyzed by double integration and yields were quantified using calibration plots prepared with Co^{II}(EDTA) (EDTA = ethylenediaminetetraacetic acid) or the tri^{t}butylphenoxyl radical.

EPR samples of CuAGAO and CoAGAO (50−150 μM) were prepared in resealable Teflon-capped tubes in an O_2-free glovebox and analyzed prior to reduction with either stoichiometric or excess PEA. Subsequent reactions with H_2O_2 utilized a manual-mixing/freeze-quench procedure that allowed reactions to be probed after 10−20 s. Reactions with O_2 required exchange of the N_2 atmosphere with pure O_2. When PEA was present in a 10-fold excess over the enzyme concentration, reactions were allowed to proceed for 100−200 s before freeze-quenching. Under these conditions, Co^{II} and/or the $TPQ_{sq\bullet+}$ formed at micromolar concentrations, in yields corresponding to ∼1%, should be detectable.

The reactive TPQ_{ox} per protein subunit was used to determine the active enzyme concentrations in kinetic assays.[32]

dx.doi.org/10.1021/jp3121484 | J. Phys. Chem. B XXXX, XXX, XXX−XXX

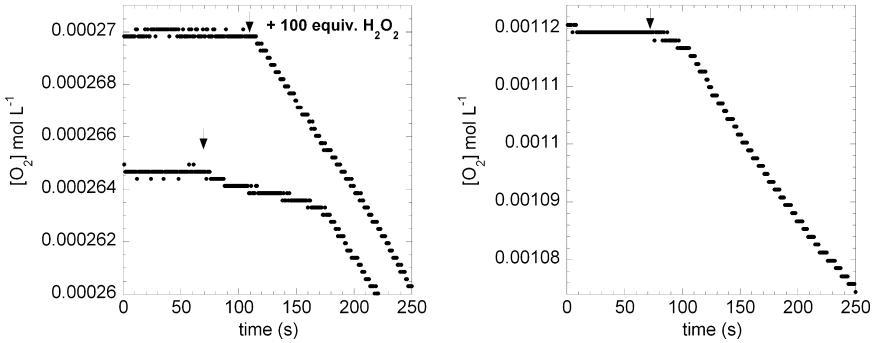

Figure 1. Time traces for CoAGAO catalyzed PEA oxidation at air saturation (a) and at O_2 saturation (b). The down-pointing arrow denotes the time at which enzyme was introduced.

Initial rates of O_2 consumption were determined with a Clark-type O_2 (YSI) electrode. In contrast to the kinetic behavior of wild-type CuAGAO,[60] CoAGAO exhibited a significant induction or lag phase. Maximal rates were estimated from the linear portion of time traces corresponding to the steepest slopes. As shown in Figure 1, the duration of the lag depended on the initial concentration of O_2 and whether the CoAGAO was pretreated with excess H_2O_2.

Oxygen isotope fractionation was analyzed as previously described[38−47,49] using a specially constructed apparatus.[64] Samples were prepared by isolating O_2 before and after treatment of O_2 saturated solutions containing PEA or BA with CuAGAO or CoAGAO. The O_2 isolated at conversions between 5 and 55% was combusted to CO_2 and the pressure determined for quantification of the fractional yield. The CO_2 samples were placed in dry glass tubes and sealed under vacuum so that they could be analyzed later using isotope ratio mass spectrometry (IRMS). IRMS was carried out on dual-inlet instruments at the University of Waterloo and Johns Hopkins University. Relative pressures and isotope fractionation results were analyzed using the Rayleigh equation: ^{18}O KIE = $\ln(R_f/R_0)/\ln(1-f)$, where R_0 is the initial ^{18}O:^{16}O ratio in the unreacted O_2 and R_f is the ^{18}O:^{16}O ratio at a specific conversion of O_2 (f). Samples analyzed at variable conversions, on time scales from seconds to hours, afforded indistinguishable results. This is particularly important in the case of CoAGAO where sample collection during the lag phase, where Co^{II} apparently undergoes oxidation to Co^{III}, could afford different results.

Crystal structures[20] of Cu^{II} and Co^{II}-containing AGAO provided initial starting points for DFT modeling. In each case, a superoxide ligand was assumed to bond to a tris-histidine coordinated metal center in an η^1-manner, displacing two or three water molecules and affording a pseudotetrahedral geometry. A hydrogen bond network was constructed with a water molecule connecting the terminal oxygen of the metal-bound superoxide and a conserved tyrosine[65] which interacts with the 4-OH of the TPQ cofactor. Reactions of $TPQ_{sq\bullet+}$ with $Cu^{II}(\eta^1\text{-}O_2^{-I})$ and $Co^{III}(\eta^1\text{-}O_2^{-I})$ were modeled with overall charges of +2 and +3, respectively, in quartet (S = 3/2) and triplet (S = 1) spin states. The reaction of TPQ_{red} with $Co^{III}(\eta^1\text{-}O_2^{-I})$ was modeled with a charge of +2 assuming a quartet spin state (S = 3/2).

All DFT calculations were performed with the *Gaussian 03* program package.[66] Geometries of reactants and transition states were optimized in the gas phase without symmetry constraints at the unrestricted *m*MPWPW91 level of theory.[67] The atomic orbital basis functions were CEP-31G (from the EMSL basis set library) for Cu and Co, 6-311G* for N and O, 6-31G for C, and STO-3G for H. To obtain accurate energies, single point corrections were applied using a triple-ζ quality basis set. The use of a larger basis set had no impact on the vibrational frequencies when calculated for an analogous reaction.[49] Gas phase Hessians were calculated at the same level of theory as the optimizations to confirm the nature of the stationary points along the reaction coordinate and to provide vibrational frequencies for the calculations of ^{18}O KIEs. All transition states possessed exactly one negative eigenvalue (i.e., imaginary mode) corresponding to the reaction coordinate.

RESULTS

Spectroscopic Characterizations of CuAGAO and CoAGAO. Metal substitution has been used to probe the mechanism(s) by which redox equivalents are transferred to O_2 via TPQ_{red} in copper amine oxidases from various sources.[25−31] In each of these works, it was assumed that the Co^{II} state persisted during enzyme turnover. Here we show that this is not the case in AGAO, where spectroscopic and kinetic evidence indicates oxidation of Co^{II} to Co^{III} by the H_2O_2 produced during enzyme turnover. Samples used in kinetic measurements were analyzed by electronic absorption and X-band EPR spectroscopy to identify the O_2 reactive form of the enzyme during catalysis. Comparison to the wild-type CuAGAO demonstrated quantification of $TPQ_{sq\bullet+}$ under rigorously anaerobic conditions. In CoAGAO, the reduced enzyme in the Co^{III} TPQ_{red} state would be expected to equilibrate with Co^{II} $TPQ_{sq\bullet+}$. Only the former species is observable, however, because of the redox potentials associated with the $TPQ_{sq\bullet+}$ and tris-histidine coordinated Co^{III} in AGAO.

The electronic absorption spectrum of CuAGAO, in the Cu^{II} TPQ_{ox} resting state, is characterized by a broad band in the visible region due to the quinone form of the cofactor ($\varepsilon_{480\ nm}$ = 2.5 × 10^3 M^{-1} cm^{-1}).[32] Treatment of this sample with PEA resulted in a rapid equilibrium between Cu^{II} TPQ_{red} and the Cu^{I} $TPQ_{sq\bullet+}$ (Figure 2a,b). Added H_2O_2 had no impact on this reaction. The $TPQ_{sq\bullet+}$ dominates the spectrum ($\varepsilon_{462\ nm}$ = 4.5 × 10^3 M^{-1} cm^{-1}) and exhibits characteristic vibrational fine structure.[68]

No $TPQ_{sq\bullet+}$ is detectable upon treating the enzyme initially containing Co^{II} TPQ_{ox} with PEA and H_2O_2 under conditions identical to those outlined for CuAGAO. Under these conditions, TPQ_{ox} disappears and a featureless spectrum with λ_{max} tailing from the UV range appears in its place (Figure 2c,d). This result reflects reduction of TPQ_{ox} to TPQ_{red} by two protons and electrons. The conversion of Co^{II} to Co^{III} by H_2O_2 is undetectable optically.

dx.doi.org/10.1021/jp3121484 | J. Phys. Chem. B XXXX, XXX, XXX−XXX

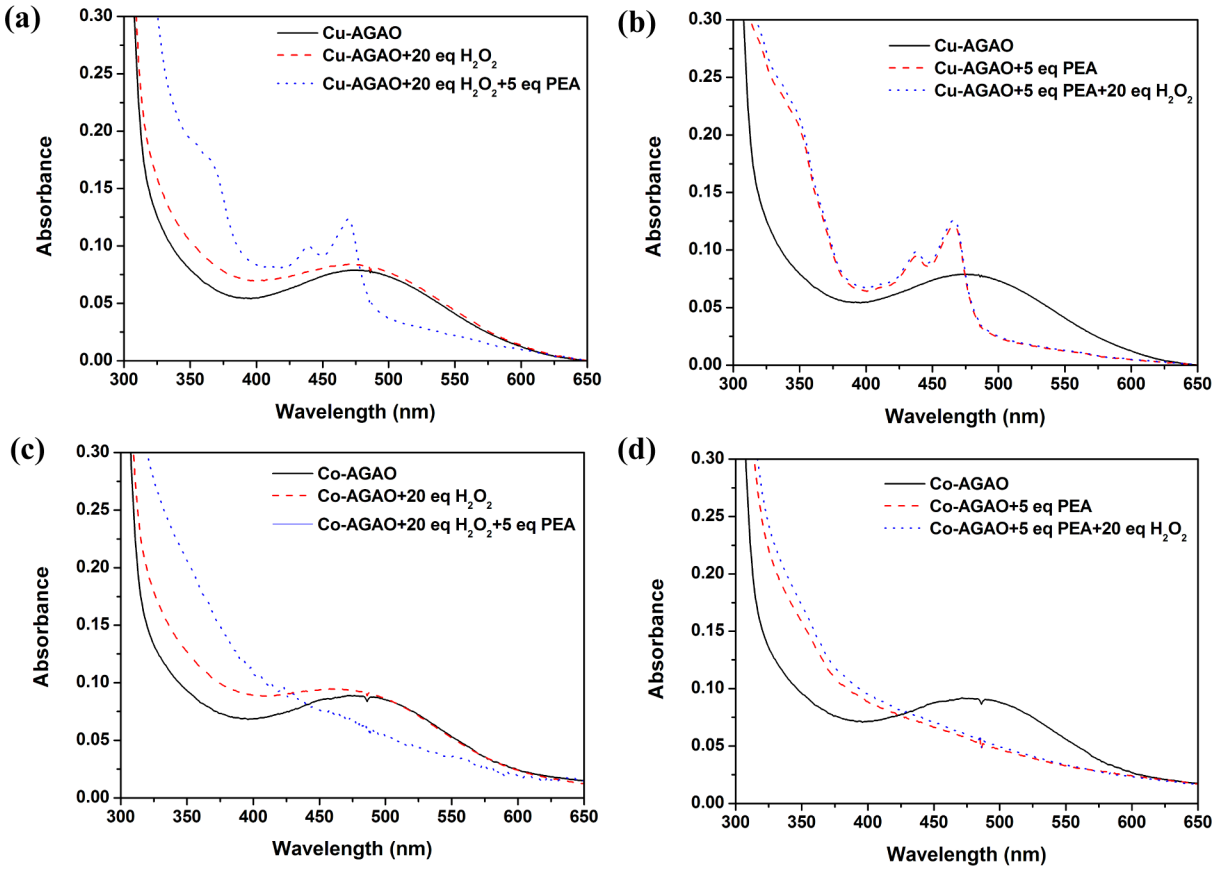

Figure 2. Anaerobic UV−vis spectra recorded at pH 7.2 and 22 °C. The Cu^{II} TPQ_{ox} AGAO was reacted with 20 equiv. of H_2O_2 followed by 5 equiv. of PEA (a) or 5 equiv. of PEA followed by 20 equiv. of H_2O_2 (b); the Co^{II} TPQ_{ox} AGAO was reacted with 20 equiv. of H_2O_2 followed by 5 equiv. of PEA (c) or 5 equiv. of PEA followed by 20 equiv. of H_2O_2 (d).

The TPQ_{red} persists in the presence of Co^{III} as indicated by EPR analysis, where treatment of Co^{II} TPQ_{ox} or Co^{II} TPQ_{red} with H_2O_2 rapidly consumes one reducing equivalent from the cobaltous ion and a second electron from an unidentified site on the surrounding protein. The only observation is the disappearance of the characteristic high-spin Co^{II} EPR signal.[61−63] Importantly, there is no detectable loss of activity or diminution in $k_{cat}/K_M(O_2)$ upon treating CoAGAO or CuAGAO with H_2O_2. In addition, added H_2O_2 causes disappearance of the lag phase, where Co^{II} is oxidized to Co^{III}, as detailed in the Experimental section.

X-band EPR experiments performed at 4 K on the isolated Co^{II} TPQ_{ox} afforded a high-spin signal due to Co^{II} (Figure 3a).[60−63] Treating the enzyme containing Co^{II} TPQ_{ox} with PEA gives Co^{II} TPQ_{red}. Warming the sample to 91 K results in characteristic disappearance of the high-spin Co^{II} state (Figure 3b).[63] When CuAGAO is treated with PEA under similar conditions, Cu^{II} TPQ_{ox} converts to an ∼1:1 mixture of Cu^{II} TPQ_{red} and Cu^{I} $TPQ_{sq\bullet+}$, where the $TPQ_{sq\bullet+}$ dominates the EPR spectrum. A broad signal is observed at 77 K which sharpens, revealing hyperfine coupling to the methylene protons, at 295 K (Figure 3c,d).[20,21] Treating the CuAGAO sample with 10 equiv. of H_2O_2, before or after the addition of PEA, has no impact on the outcome of these experiments.

An anaerobic solution of CoAGAO, pretreated with excess PEA, is depicted in Figure 4a,c. The ^{59}Co hyperfine interaction is best resolved at 18 K. The sample was subsequently treated with 10 equivalents of H_2O_2 followed by rapid mixing and freezing within 10−20 s (Figure 4b) or reacted with excess O_2 and allowed to react for 100−200 s at ambient temperature (Figure 4d). In both experiments, ∼98% of the high-spin Co^{II} signal converted into an EPR silent species, most likely Co^{III}. At the same time, a minor signal corresponding to <0.2% of the integrated area increased to approximately 2%. Subsequent oxygenation of the sample had no discernible effect on the EPR spectrum. This minor species could be the Co^{III} (η^1_O_2^{-I})[69] or an O_2-inert low-spin Co^{II} species, which may or may not be bound to AGAO.

Rate Limiting Step in Enzyme Catalysis. Like CuAGAO,[21] CoAGAO reacts by a simple "ping-pong" or "double displacement" kinetic mechanism in this and other studies.[25−31] Thus, $k_{cat}/K_M(O_2)$ is independent of the concentration of the primary amine cosubstrate and k_{cat}/K_M(PEA) or k_{cat}/K_M(BA) is independent of the O_2 concentration. A significant substrate deuterium kinetic isotope effect was observed on the turnover-limiting rate-constant ($^Dk_{cat}$) with CuAGAO. Initial studies of protio-BA compared to α,α-d_2-BA indicated $^Dk_{cat}$ = 2.3 ± 0.1 and $^Dk_{cat}/K_M$(BA) = 9.4 ± 0.4, at pH 7.2 and O_2 saturation. These data suggest that k_{cat} is additionally influenced by a partially rate-limiting reaction during the reduction of O_2 (cf. eq 2).

PEA was used to compare the O_2 reactivity of CuAGAO and CoAGAO because the turnover rates with this substrate were greater than those with BA. The steady-state kinetics for CuAGAO reacting with O_2 at saturating PEA concentration indicates $K_M(O_2)$ = 27 ± 2 μM and k_{cat} = 38 ± 0.6 s^{-1} at pH 7.2. These results agree with those previously reported under similar conditions.[21] The pH and pD ranges were expanded

dx.doi.org/10.1021/jp3121484 | J. Phys. Chem. B XXXX, XXX, XXX−XXX

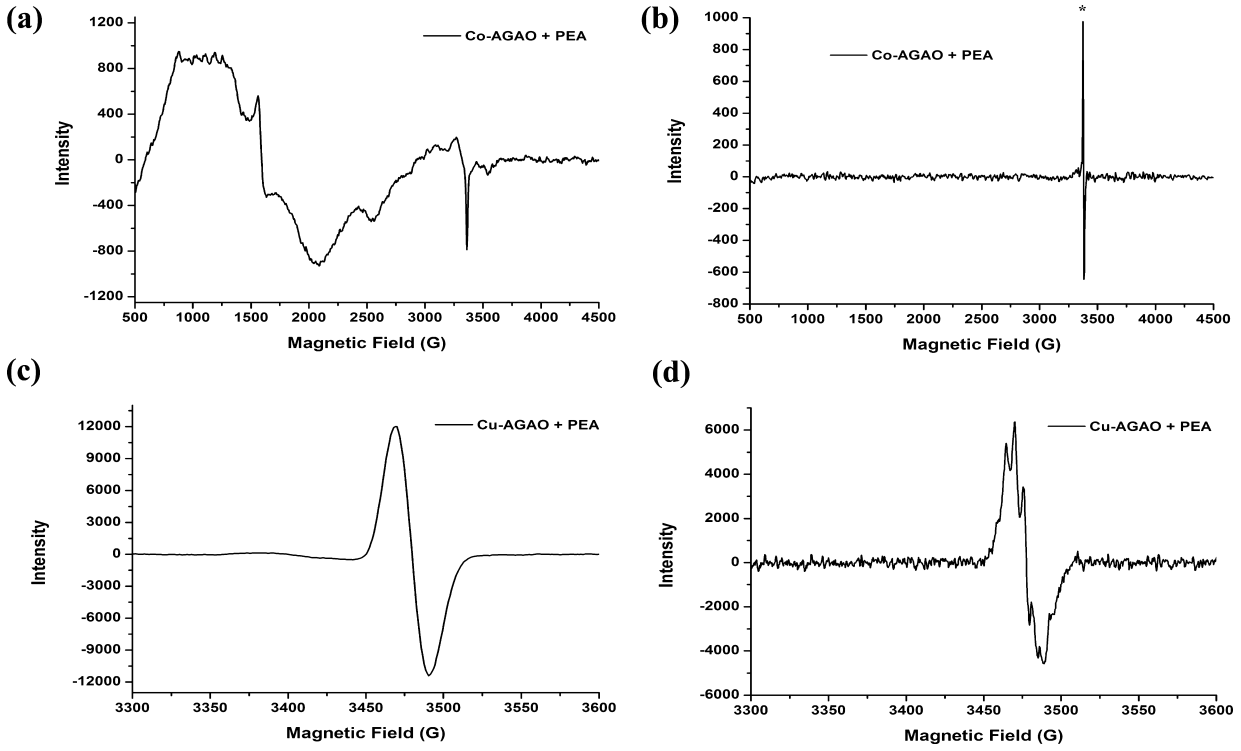

Figure 3. Anaerobic X-band EPR spectra at pH 7.2. Co^{II} TPQ_{ox} AGAO (140 μM) reacted with PEA (2 mM) was observed at 4 K (a) and at 91 K (b); Cu^{II} TPQ_{ox} AGAO (100 μM) reacted with PEA (400 μM) was observed at 77 K (c) and at 295 K (d). The * corresponds to an organic radical impurity. The parameters used to record EPR spectra are summarized in the Experimental Section.

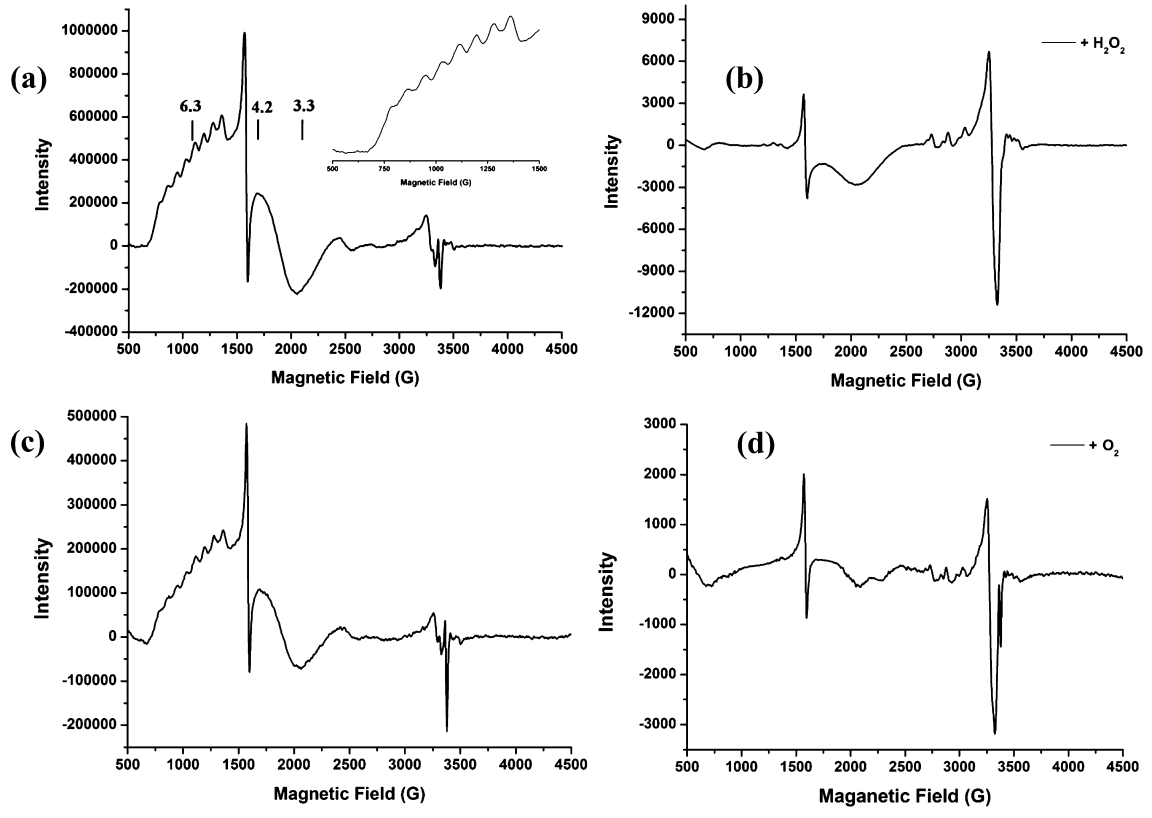

Figure 4. Anaerobic X-band EPR spectra acquired at 18 K. The PEA-reduced CoAGAO (50 μM) exhibits eight-line hyperfine splitting due to ^{59}Co, $I = 7/2$ (a). This anaerobic sample was treated with 10 equiv. of H_2O_2 resulting in disappearance of >98% of the Co^{II} signal (b). Similar results were obtained when CoAGAO (150 μM) was prereduced with 10 equiv. of PEA (c) and then reacted with excess O_2 at ambient temperature (d). Acquisition parameters are tabulated in the Experimental Section.

dx.doi.org/10.1021/jp3121484 | J. Phys. Chem. B XXXX, XXX, XXX−XXX

here and measurements made with CuAGAO or CoAGAO. In the latter, $K_M(O_2)$ is immeasurably large (>1.4 mM), precluding determination of the limiting k_{cat}.

Kinetic data were collected to determine the contribution of proton transfer to k_{cat} for the wild-type CuAGAO in Figure 5.

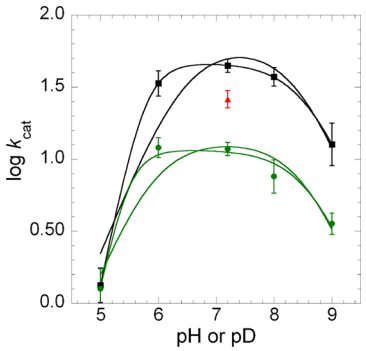

Figure 5. Variation of k_{cat} with pH and pD for CuAGAO reacting with protio-PEA in H_2O (black squares) and $\alpha,\alpha,\beta,\beta$-$d_4$-PEA in D_2O (green circles). The result for CuAGAO reacting with protio-PEA in D_2O is also shown (red triangle). The data are better fitted to a one-state/three pK_a model: $\log(k_{cat}) = \log(k_{cat})_{max} - \log(1 + 10^{pKa1-pH} + 10^{pKa1+pKa2-2\times pH} + 10^{pH-pKa3})$ than a one-state/two-pK_a model: $\log(k_{cat}) = \log(k_{cat})_{max} - \log(1 + 10^{pKa1-pH} + 10^{pH-pKa2})$.

Oxidation of per-protio PEA in H_2O compared to the $\alpha,\alpha,\beta,\beta$-$d_4$-PEA in D_2O as the pH and pD was raised from 5.0 to 9.0 revealed that the isotope effect, $^Dk_{cat}$, increased from 1.1 to 4.9 and then decreased to 3.5. A solvent KIE of ~2 was determined on the reaction of protio-PEA in H_2O and D_2O. These results suggest the presence of at least two isotopically sensitive steps. One is associated with the C−H(D) cleavage step during amine oxidation.[32] The other isotopic step appears to occur during O_2 reduction. Further analysis of the $^Dk_{cat}/K_M(O_2)$ was, therefore, undertaken with selectively labeled and unlabeled PEA (vide infra).

Despite the kinetic complexity of k_{cat} with CuAGAO the pH and pD profiles can be described using two different multiparameter fits that reflect one reactive state and either two or three autoionization processes. Fitting the data in Figure 5 to a two pK_a model indicates a bell-shaped curve characterized by pK_{a1} = 6.4 ± 0.4 and pK_{a2} = 8.4 ± 0.5 for protio PEA in H_2O and pK_{a1} = 5.9 ± 0.3 and pK_{a2} = 8.5 ± 0.3 for d_4-PEA in D_2O. Fitting the same data to a three pK_a model gives a somewhat distorted profile with a better fit to pK_{a1} = 4.8 ± 0.2, pK_{a2} = 6.7 ± 0.2, and pK_{a3} = 8.5 ± 0.1 for protio PEA in H_2O and a pK_{a1} = 5.1 ± 2.0, pK_{a2} = 5.8 ± 2.5, and pK_{a3} = 8.7 ± 0.4 for d_4-PEA in D_2O. The high and low pK_a values exhibit shifts consistent with equilibrium solvent isotope effects, while the intermediate pK_a is more difficult to interpret.

Steady State Kinetics of O_2 Reduction. Solvent and substrate deuterium KIEs were determined upon the steady-state rate constant, $k_{cat}/K_M(O_2)$, at variable pH and pD for CuAGAO and CoAGAO. Under the assay conditions, the substrate amine reacts with the Cu^{II} or Co^{III} TPQ_{ox} containing enzyme. Use of the labeled d_4-PEA results in retention of a deuteron within the active site. It can be concluded that this hydrogen is subsequently recycled during enzyme turnover where it partitions into the 4-hydroxyl of the TPQ cofactor. In the presence of O_2, hydrogen is transferred to the terminal oxygen of the $Cu^{II}(\eta^1-O_2^{-I})$ or $Co^{III}(\eta^1-O_2^{-I})$ giving rise to a substrate deuterium kinetic isotope effect on η^1-hydroperoxide formation.

Bimolecular rate constants corresponding to O_2 reduction by CuAGAO and CoAGAO, with unlabeled and labeled PEA, are shown at variable pH and pD in Figure 6. The data for

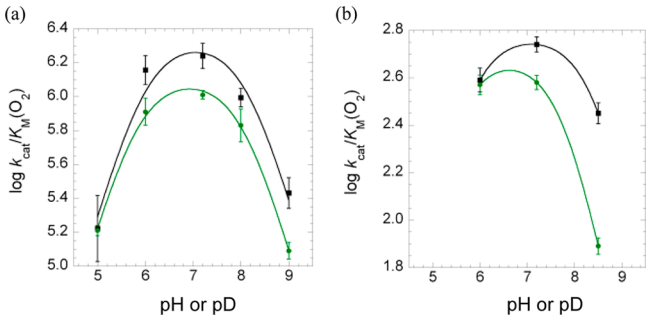

Figure 6. Profiles of $k_{cat}/K_M(O_2)$ at variable pH (black squares) and pD (green circles) for CuAGAO (a) and CoAGAO (b) fitted to one-state/two-pK_a models: $\log(k_{cat}) = \log(k_{cat})_{max} - \log(1 + 10^{pKa1-pH} + 10^{pH-pKa2})$.

CuAGAO fitted to a one-state/2 pK_a model indicates autoionization constants of ~6 and 8. A similar result is obtained for CoAGAO based on fewer data. The pH and pD profiles resemble those seen for k_{cat} in Figure 5, yet the most acidic pK_a, assigned to the active-site aspartate, which mediates proton transfer during the reductive half-reaction, has vanished.[32]

The $^Dk_{cat}/K_M(O_2)$ measured with labeled d_4-PEA, suggests that the pK_a of 6−7 may be attributed to the 4-OH of the $TPQ_{sq\bullet+}$, while the pK_a ca. 8−9 could be attributed to the putative $Cu^{II}OOH$ or $Co^{III}OOH$ product. This η^1-hydroperoxide species is expected to hydrogen bond to an active site water, which connects the conserved tyrosine hydrogen bonded to the 4-OH of the $TPQ_{sq\bullet+}$ (or TPQ_{red}, vide infra). The proton affinities of the partially reduced cofactor and the putative η^1-superoxide intermediate are expected to contribute to the thermodynamics of PCET and thereby influence $k_{cat}/K_M(O_2)$. A caveat to this interpretation is that steady-state kinetic data do not always reflect intrinsic pK_a values in proteins.[38]

The pH and pD profiles obtained with protiated PEA in H_2O and $\alpha,\alpha,\beta,\beta$-$d_4$-PEA in D_2O suggest isotope effects on $k_{cat}/K_M(O_2)$ of 1.7 ± 0.1 in CuAGAO and 1.4 ± 0.1 in CoAGAO at the pH and pD optima. In contrast, a negligible solvent KIE of ~1.1 determined by reacting CuAGAO with protio PEA in D_2O. This result is consistent with retention of deuterium due to a kinetically slow solvent isotope exchange with hydroxylic residues in the active site.[39,70,71] The substrate deuterium KIE on $k_{cat}/K_M(O_2)$ is indicative of rate-limiting PCET, where the proton transfers at the same time as the electron.[72] Based on the crystal structures,[20] this reaction proceeds over ~6 Å from the $TPQ_{sq\bullet+}$ (or TPQ_{red}) to the formally $Cu^{II}-O_2^{-I}$ or $Co^{III}-O_2^{-I}$ adduct.

Measurements of Competitive O-18 Kinetic Isotope Effects. Competitive ^{18}O KIEs were measured as described in the Experimental section. Samples obtained from experiments at variable consumptions of the initial O_2 present (5 to 55%) at concentrations from 270 μM to ~1.3 mM, were analyzed by IRMS. The isotope fractional plots, shown in Figure 7, correspond to normal ^{18}O KIEs where the light isotopologue ($^{16,16}O_2$) reacts faster than the heavier one ($^{16,18}O_2$). The ^{18}O

dx.doi.org/10.1021/jp3121484 | J. Phys. Chem. B XXXX, XXX, XXX−XXX

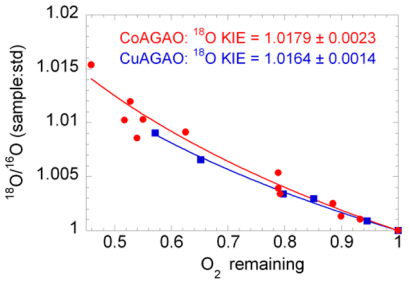

Figure 7. Oxygen isotope fractionation by CuAGAO (blue squares) and CoAGAO (red circles) fitted to the Rayleigh equation given in the Experimental Section.

KIEs were indistinguishable when PEA or BA served as the reducing cosubstrate.

The nearly indistinguishable isotope fractionation patterns for CuAGAO and CoAGAO indicate ^{18}O KIEs of 1.0164 ± 0.0014 and 1.0179 ± 0.0023, respectively. These values are the same within the experimental error, consistent with the similar deuterium KIEs on $k_{cat}/K_M(O_2)$. This result implies that the enzymes react by identical mechanisms. This result is striking, because of the 10^3-fold variation in $k_{cat}/K_M(O_2)$. This effect is proposed to derive from a large difference in a pre-equilibrium formation of the Cu^I and Co^{II} $TPQ_{sq\bullet+}$ states which precede the reversible formation of the Cu^{II} or Co^{III} η^1-superoxide intermediates that subsequently undergo rate-limiting PCET.

Oxygen Isotope Effects Derived from DFT Calculations. Experimental ^{18}O KIEs are compared to theoretically predicted values derived from DFT calculations on energy minimized transition state structures derived from reactions of substrate-reduced CuAGAO and CoAGAO with $^{16,16}O_2$ and $^{16,18}O_2$. The calculations assumed that the enzymes react through tris-histidine coordinated $Cu^{II}(\eta^1-O_2^{-I})$ and $Co^{III}(\eta^1-O_2^{-I})$ intermediates.[38,60] Using the calibrated DFT protocol, transition states were located for PCET to metal O_2-adducts engaged in extensive hydrogen bonding to the $TPQ_{sq\bullet+}$. Substitution of TPQ_{red} for the $TPQ_{sq\bullet+}$ was considered as well to represent the possibility that Co^{II} is not oxidized by H_2O_2 during enzyme turnover.

The transition states located from defined precursor states, possessed exactly one imaginary mode with a frequency in the range of 1230i to 800i cm^{-1}.[60] As expected, these values are intermediate between the O−O vibrations of the η^1-dioxygen/superoxide reactant and η^1-hydroperoxide product structures. All isotopic vibrational frequencies were used in the analysis of ^{18}O KIE_{calc}, without scaling or correction for anharmonicity. Intramolecular isotope effects computed from Boltzmann weighting factors were ten times smaller than the measured effects and, therefore, within the experimental errors.

The measured and calculated ^{18}O KIEs are compared to the natural abundance oxygen-18 equilibrium isotope effects (^{18}O EIEs) computed for isolated tris-methylimidazole-coordinated Cu^{II} and Co^{III} complexes with η^1-superoxide ligands.[38,60] The same unrestricted *m*PWPW91 functional along with the atomic basis functions quoted in the Experimental Section were used. This approach has been shown to reproduce temperature-dependent ^{18}O EIEs on η^1-O_2 binding to a variety of transition metal complexes, including Cu(I) and Co(II).[56,57] The resulting ^{18}O EIE_{calc} = 1.0104 for $Cu^{II}(\eta^1-O_2^{-I})$ and 1.0036 for $Co^{III}(\eta^1-O_2^{-I})$ are smaller than the ^{18}O KIEs defined by eq 4. This is the result of normal mass effect on the imaginary mode describing the reaction coordinate and on the pseudoequilibrium describing the transition state. The latter term is the product of a normal entropic isotope effect on O_2 binding and an inverse enthalpic isotope effect on the reduction of O_2 to the level of O_2^{-II}.

DISCUSSION

Characterization of Cu and Co-Reconstituted AGAO. The "oxidized" active sites of Cu^{II} and Co^{II}-containing AGAO have been characterized by X-ray crystallography and the structures are depicted in Figure 8.[20] More relevant to this study are the active-sites of the substrate-amine reduced enzymes, which react with O_2. The reduced CuAGAO has been characterized and shown to contain tricoordinate Cu^I.[73] The analogous substrate-reduced CoAGAO has not been characterized but it is likely to have a higher coordination number in view of the three aqua ligands in the Co^{II} structure.[20]

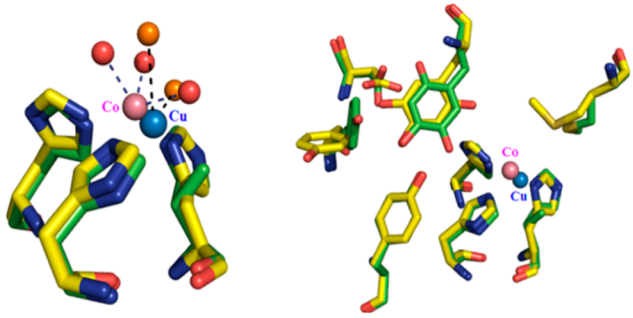

Figure 8. Active sites of the fully oxidized forms of CuAGAO and CoAGAO superimposed.[20]

For simplicity, pseudotetrahedral geometries composed of $Cu^{II}(\eta^1-O_2^{-I})$ or $Co^{III}(\eta^1-O_2^{-I})$ and three histidine ligands are compared computationally within the active site of AGAO. Optimization at the density functional level of theory afforded the network of hydrogen bonds conducive to PCET. Specifically, the terminal oxygen of the η^1-superoxide was connected to one water molecule which was hydrogen-bonded to the conserved tyrosine[65] that interacts with the 4-OH of the $TPQ_{sq\bullet+}$ (or TPQ_{red}).

Comparisons of Copper Amine Oxidase to Cobalt-Substituted Variants. Previous studies have suggested similarities between the prokaryotic AGAO and the eukaryotic enzyme from pea seedlings (PSAO).[33,38] PSAO exhibits high homology and similar reactivity to the enzyme from lentil seedlings (LSAO).[74−76] Treatment of LSAO and PSAO with an excess of primary amine under anaerobic conditions leads to the Cu^I $TPQ_{sq\bullet+}$ state in 70−80% yield at pH 7.2. The equilibrium is only slightly less favorable in AGAO where Cu^I $TPQ_{sq\bullet+}$ is formed in ∼50% yield under the same conditions. Importantly, the concentration of neither Cu^I $TPQ_{sq\bullet+}$ nor the Cu^{II} TPQ_{red} precursor had any effect on $k_{cat}/K_M(O_2)$. Thus, rapid, reversible electron transfer, followed by reversible O_2 binding, occurs before the rate-limiting step. Time-resolved studies of AGAO[17,22] have demonstrated that the Cu^I $TPQ_{sq\bullet+}$ is kinetically competent to reduce O_2 during amine oxidase catalysis. The enzymes containing Co^{II} (or Co^{III}) in place of Cu^{II} exhibit a $>10^3$-fold diminution in $k_{cat}/K_M(O_2)$.

^{18}O KIEs have previously been measured on reactions of PSAO[38] as well as the structurally related copper amine oxidases from bovine serum (BSAO)[44] and the yeast *Hansenula polymorpha* (HPAO).[29,41] Moderately sized normal isotope

dx.doi.org/10.1021/jp3121484 | J. Phys. Chem. B XXXX, XXX, XXX−XXX

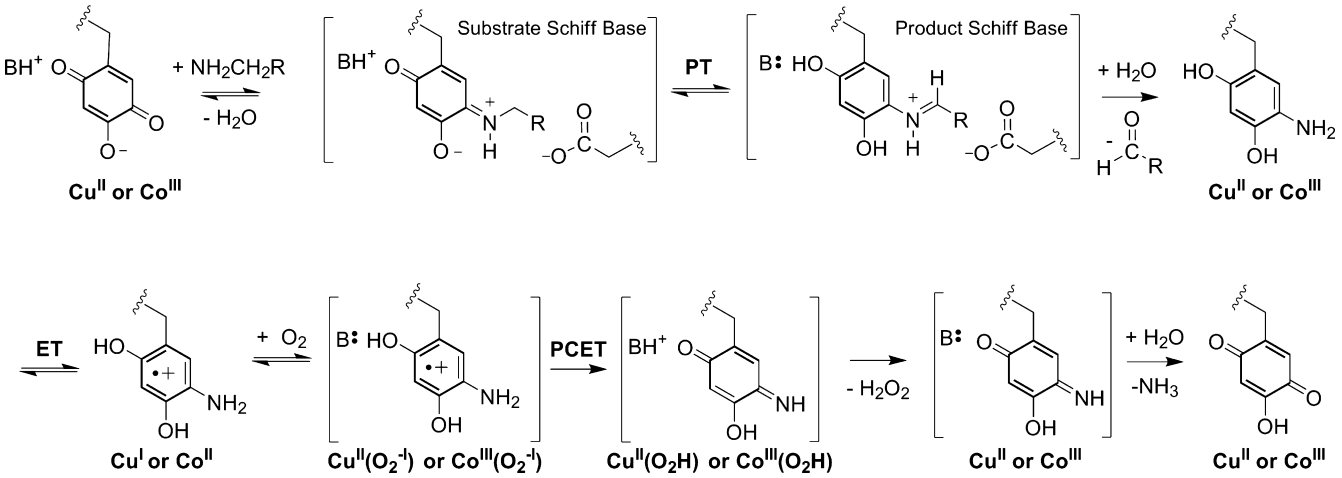

Figure 9. Reductive and oxidative phases of catalysis in CuAGAO and CoAGAO. Catalyzed steps include proton transfer (PT), electron transfer (ET), and proton-coupled electron transfer (PCET).

Scheme 1. Mechanisms of O_2 Reduction by CuAGAO and CoAGAO

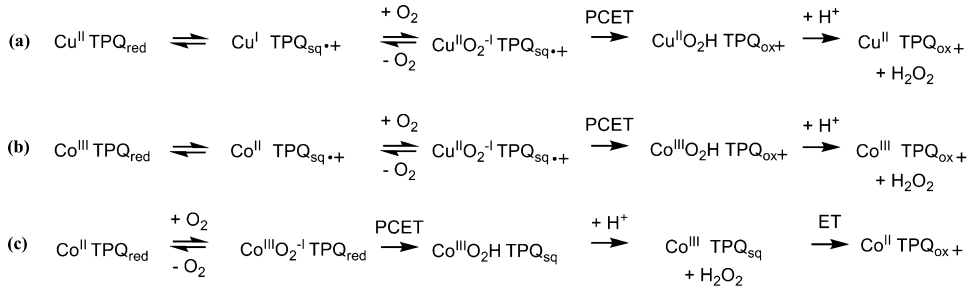

effects were observed, falling within a narrow range of 1.0074 to 1.0136. These results are difficult to reconcile with earlier proposals of O_2 reduction by outer-sphere electron transfer directly from TPQ_{red} in the rate-limiting step.[28,29] This reaction would produce $O_2^{\bullet-}$ and $TPQ_{sq\bullet+}$ without affecting the redox state of the active site metal. For such reactions, relegated to react by outer-sphere electron transfer, ^{18}O KIEs have been measured and calculated to be ~1.028 ± 0.002 over a range of free energies (ΔG°).[45−47] An alternative, wherein O_2 is reduced to $O_2^{\bullet-}$ reversibly, prior to η^1-superoxide coordination to the metal cannot be excluded;[37] however, this mechanism blurs the distinction between inner-sphere and outer-sphere electron transfer.

CuAGAO and CoAGAO exhibit indistinguishable ^{18}O KIEs that fall just outside the range determined for the structurally homologous copper amine oxidases mentioned above. These findings must be reconciled with steady-state kinetics which reveal that $K_M(O_2)$ is greatly elevated in CoAGAO relative to CuAGAO. The $K_M(O_2)$ reflects all reversible steps preceding the proposed rate-limiting PCET, where proton and electron translocations occur over a relatively large distance.[72] The spectroscopic data summarized above suggest that the difference in $K_M(O_2)$ relates to the $Co^{III/II}$ redox potential, which is significantly more negative than the $Cu^{II/I}$ redox couple. As a result, $Co^{III}(\eta^1{-}O_2^{-I})$ $TPQ_{sq\bullet+}$ is destabilized relative to $Cu^{II}(\eta^1{-}O_2^{-I})$ $TPQ_{sq\bullet+}$. Thus, the thermodynamics are expected to reduce the free energy barrier ($\Delta G^{\ddagger}$) for $Co^{III}(\eta^1{-}O_2H)$ TPQ_{ox+} formation relative to the $\Delta G^{\ddagger}$ for $Cu^{II}(\eta^1{-}O_2H)$ TPQ_{ox+} formation in the rate-limiting step. The DFT modeling described below provides compelling evidence that the ^{18}O KIEs are determined by similar transition states involving long-range unidirectional PCET.

Figure 9 depicts ground state structures and intermediates formed during the catalytic cycle of AGAO. Initially, condensation of the primary amine with the TPQ_{ox} cofactor forms a "substrate" Schiff base intermediate. This species undergoes deprotonation by the active site aspartate residue to form a "product" Schiff-base intermediate. Hydrolysis affords an aldehyde along with the TPQ_{red}, which is the aminoresorcinol form of the cofactor that reacts with O_2. The 5-NH_2 makes the 4-OH less acidic than in the parent TPQ and, therefore, TPQ_{red} is expected to undergo electron transfer to produce $TPQ_{sq\bullet+}$ along with Cu^I or Co^{II}. Subsequent coordination of O_2 to the reduced metal generates $Cu^{II}(\eta^1{-}O_2^{-I})$[36,56] or a similar $Co^{III}(\eta^1{-}O_2^{-I})$ species,[57] capable of abstracting the equivalent of a hydrogen atom from the $TPQ_{sq\bullet+}$.[69,77] An η^1-hydroperoxide intermediate is formed, together with an iminoquinone intermediate, where the extra proton is shown attached to a nearby base. Protonolysis produces H_2O_2 and hydrolysis of the iminoquinone causes the extrusion of NH_3.

In Figure 9, the $Cu^{II}(\eta^1{-}O_2^{-I})$ and $Co^{III}(\eta^1{-}O_2^{-I})$ intermediates undergo PCET with the $TPQ_{sq\bullet+}$ ~6 Å away. The analogous reaction with the TPQ_{red} is expected to be less favorable because of the greater bond strength of the 4-OH. On these grounds, the reaction of the TPQ_{red} is expected to exhibit a larger $\Delta G^{\ddagger}$ than the reaction of the $TPQ_{sq\bullet+}$. This proposal is in line with the relatively small rate constant observed during the induction phase where $Co^{III}(\eta^1{-}O_2^{-I})$ reacts with TPQ_{red}.

In this study, we have shown through EPR experiments and steady-state kinetics, that Co^{II} is oxidized to Co^{III} upon exposure to H_2O_2. The source of the second reducing

dx.doi.org/10.1021/jp3121484 | J. Phys. Chem. B XXXX, XXX, XXX−XXX

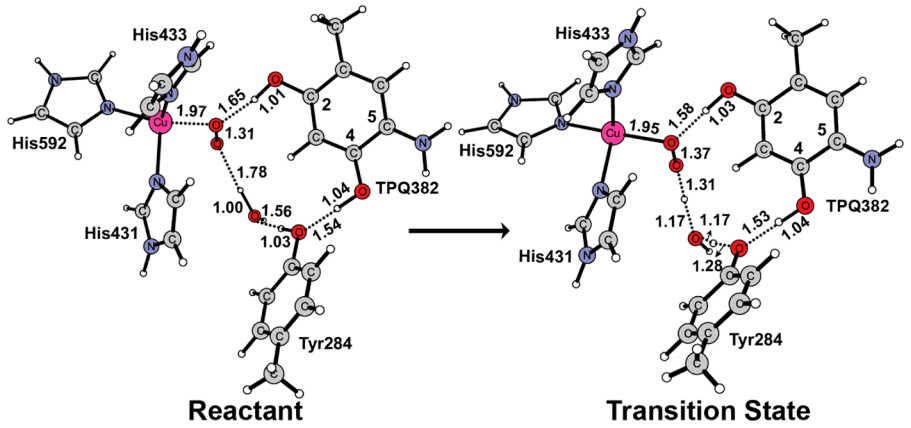

Figure 10. PCET reaction of $Cu^{II}(\eta^1-O_2^{-I})$ with $TPQ_{sq\bullet+}$ along a quartet energy surface.

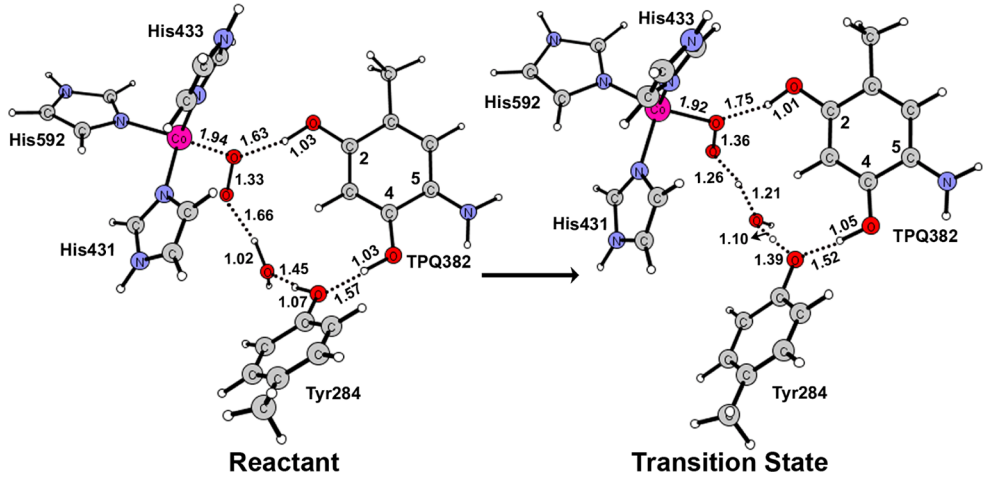

Figure 11. PECT reaction of $Co^{III}(\eta^1-O_2^{-I})$ with $TPQ_{sq\bullet+}$ along a triplet energy surface.

equivalent has not been identified, although the tyrosine residues in proximity to the metal cofactor are likely donors. Rates used in the kinetic analysis were measured either after the induction phase was complete or by pretreating the enzyme with 10 equivalents of H_2O_2. The latter removed the induction phase and ensured determination of the maximum $k_{cat}/K_M(O_2)$.

Reconstitution of the AGAO apoprotein with Ni^{II} or Zn^{II}, using the same protocol developed for Co^{II}, greatly diminishes the rates of enzymatic O_2 reduction such that they are difficult to resolve over the background.[20] Similar behavior occurs in the cobalt-containing amine oxidase from *E. coli* (ECAO)[26] as well as PSAO,[25] LSAO,[30] BSAO,[31] and HPAO.[28] In HPAO, perturbation of a nonmetal binding site on the protein is believed to inhibit $O_2^{\bullet-}$ formation by outer-sphere electron transfer.[78] The results reported in this study provide a new frame of reference for understanding the compromised rates of O_2 reduction by the AGAO containing Co^{III} TPQ_{red} rather than Co^{II} TPQ_{red}.

Computational Analysis of Reaction Mechanisms. The reactions in Scheme 1a,b accommodate the nearly superimposable pH and pD profiles as well as the deuterium KIEs observed with $\alpha,\alpha,\beta,\beta$-$d_4$-PEA in CuAGAO and CoAGAO. The measured ^{18}O KIEs are indistinguishable within experimental error, indicating that $k_{cat}/K_M(O_2)$ is controlled by the same rate-limiting PCET step. The aggregate results support the mechanisms depicted in Scheme 1a,b (over that shown in Scheme 1c).

DFT calculations were used to evaluate the transition states for $Cu^{II}(\eta^1-O_2^{-I})$ and $Co^{III}(\eta^1-O_2^{-I})$ reduction. Although earlier DFT studies focused on the mechanism of O_2 reduction by copper amine oxidases,[79,80] the first redox step was considered rate-limiting rather than the second[28,29] and none of the calculations attempted to model the ^{18}O KIEs as a means of validation. In this study, transition state calculations reproduce experimental ^{18}O KIEs with a high level of agreement, providing the evidence needed to evaluate the specific mechanisms of reaction with O_2. As mentioned above, the ^{18}O KIEs determined in this study are significantly smaller than those expected for the reduction of O_2 to $O_2\bullet-$ by outer-sphere electron transfer.[37,45−47] The first irreversible step is proposed to be PCET, following pre-equilibrium formation of the $Cu^{II}(\eta^1-O_2^{-I})$ $TPQ_{sq\bullet+}$ and $Co^{III}(\eta^1-O_2^{-I})$ $TPQ_{sq\bullet+}$ adducts, for which the corresponding ^{18}O EIEs were estimated to be 1.0104 and 1.0036, respectively. The transfer of electron and proton originating from the $TPQ_{sq\bullet+}$, connected to the η^1-superoxide ligand through a network of hydrogen bonds, causes elevation of the ^{18}O KIEs.

The oxidative mechanisms of CuAGAO and CoAGAO are formulated in Scheme 1. In Scheme 1a, the $Cu^{II}(\eta^1-O_2^{-I})$ which exists as a triplet ground state due to ferromagnetic coupling of two unpaired electrons.[56] This state is assumed to interact with the doublet state of the $TPQ_{sq\bullet+}$, resulting in a quartet energy surface. The associated transition state for

dx.doi.org/10.1021/jp3121484 | J. Phys. Chem. B XXXX, XXX, XXX−XXX

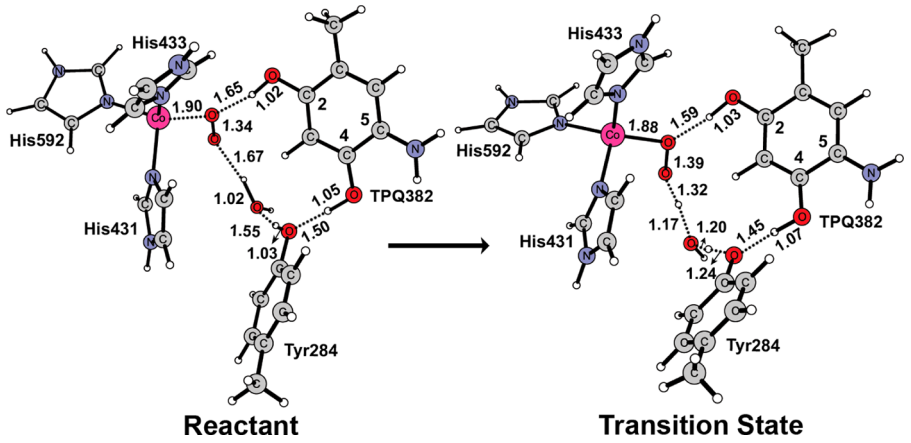

Figure 12. PCET Reaction of $Co^{III}(\eta^1-O_2^{-I})$ with TPQ_{red} along a quartet energy surface.

PCET is shown in Figure 10 where the calculated $\Delta G^{\ddagger}$ = 7.9 kcal mol^{-1} in the gas phase.

The computed reaction coordinate reveals that the $Cu^{II}-O$ bond distance contracts from 1.97 to 1.95 Å as the O−O bond length expands from 1.31 to 1.37 Å. The transition state is characterized by isotopically sensitive imaginary frequencies ranging from 1231.20i and 1227.84i cm^{-1} for the $^{16}O-^{16}O$ and $^{18}O-^{18}O$ isotopologues, respectively. The imaginary modes give rise to a normal $^{18}\nu_{RC}$ while the stable modes give rise to a normal $^{18}K_{TS}$, which together amount to an ^{18}O $KIE_{calc} \approx 1.013$ for the reaction of the light (16,16) relative to the mixed (16,18) isotopologues (cf. eq 4).[60] The ^{18}O KIE_{calc} derived from gas phase frequencies is in good agreement with the experimental ^{18}O KIE = 1.0164 ± 0.0014. Further, the ^{18}O KIE_{calc} is unchanged by inclusion of the intramolecular isotope effect, arising from the slight preference for ^{18}O bonding to Cu and ^{16}O bonding to H.

A similar transition state characterizes CoAGAO. Scheme 1b represents the case in which H_2O_2 produced during catalytic turnover oxidizes Co^{II} to Co^{III} on the experimental time scale. As a result, the TPQ_{red} reduces the Co^{III} to generate a Co^{II} $TPQ_{sq\bullet+}$ intermediate capable of binding O_2. A quartet state corresponding to the ferromagnetic $Co^{III}O_2^{-I}$ is assumed by analogy with the above-mentioned ferromagnetic $Cu^{II}O_2^{-I}$. The former state can interact with the doublet state of the $TPQ_{sq\bullet+}$ resulting in a triplet energy surface. The transition state in Figure 11 is calculated to have a $\Delta G^{\ddagger}$ = 3.0 kcal mol^{-1} in the gas phase.

The metrical changes upon reduction of $Co^{III}O_2^{-I}$ by the $TPQ_{sq\bullet+}$ are somewhat smaller than those associated with reduction of $Cu^{II}O_2^{-I}$. The $Co^{III}-O$ bond distance contracts from 1.94 Å to 1.92 Å as the O−O bond undergoes a lengthening from 1.33 to 1.36 Å in the transition state. The change in $^{18}\nu_{RC}$ characterizing PCET in the transition state is also somewhat smaller. The absolute imaginary frequencies range from 802.159i cm^{-1} for the $^{16}O-^{16}O$ isotopologue to 799.213i cm^{-1} for the $^{18}O-^{18}O$ isotopologue. The product of $^{18}\nu_{RC}$ and $^{18}K_{TS}$ gives an ^{18}O $KIE_{calc} \approx 1.014$ for the reaction of light versus mixed isotopologues; this result is in reasonable agreement with the experimental ^{18}O KIE = 1.0179 ± 0.0023. The calculated value is unchanged by correction for the intramolecular isotope effect and comparable to the ^{18}O KIE_{calc} computed for the higher energy pathway described below.

The $\Delta G^{\ddagger}_{calc}$ associated with the transition state in Figure 12 is slightly larger than that computed for that in Figure 11. In Scheme 1c, the ferromagnetic Co^{III} η^1-superoxide intermediate forms upon simple O_2 coordination to Co^{II} TPQ_{red}. Considering subsequent PCET along the quartet energy surface gives a gas phase $\Delta G^{\ddagger}$ = 4.1 kcal mol^{-1} for the PCET step. The slightly elevated $\Delta G^{\ddagger}_{calc}$ is proposed to reflect the stronger 4-OH bond in TPQ_{red} relative to that in the $TPQ_{sq\bullet+}$.

In the reaction depicted in Figure 12, the $Co^{III}-O$ bond distance contracts from 1.90 to 1.88 Å as the O−O bond lengthens from 1.34 to 1.39 Å in the transition state. PCET from the 4-OH position of the TPQ_{red} exhibits a larger $^{18}\nu_{RC}$ than the reaction in Figure 11. The imaginary frequency changes from 1129.23i cm^{-1} for the $^{16}O-^{16}O$ isotopologue to 1125.94i cm^{-1} for the $^{18}O-^{18}O$ isotopologue. The $^{18}\nu_{RC}$ computed for the light versus mixed isotopologues, taken together with the corresponding $^{18}K_{TS}$, gives an ^{18}O $KIE_{calc} \approx 1.015$. This reaction is associated with an ^{18}O KIE_{calc} somewhat closer to the experimental value; however, it is computed to have a larger $\Delta G^{\ddagger}_{calc}$. Moreover, the reaction is excluded on the grounds that H_2O_2 rapidly oxidizes the Co^{II}-reconstituted AGAO on the time scale of enzyme turnover.

CONCLUSIONS

In this study, we have demonstrated that a redox-active metal is needed to catalyze reduction of O_2 to H_2O_2 in copper amine oxidases. Both Cu^{I} and Co^{II} function in this capacity, reacting with O_2 by inner-sphere electron transfer to eliminate charge buildup due to $O_2^{\bullet-}$, thereby lowering the intrinsic free energy barrier by minimizing the outer-sphere reorganization energy.[46] The active site metal ion also facilitates long-range proton-coupled electron transfer to prebound O_2 through a network of hydrogen bonds. The main evidence for this reaction comes from similar competitive ^{18}O KIEs and deuterium KIEs on the second order rate constants for O_2 consumption by the substrate-reduced CuAGAO and CoAGAO. These observations were reproduced by the DFT calculations.

At the pH optima, enzymic rate constants of 1.4 × 10^6 $M^{-1}s^{-1}$ (CuAGAO) and 5.5 × 10^2 $M^{-1}s^{-1}$ (CoAGAO) are orders of magnitude greater than those observed in TPQ model systems.[81−83] The primary influence on catalysis is thus reasoned to be O_2 binding to the reduced transition metal. The 10^3-fold disparity for CuAGAO and CoAGAO is attributed to formation of Cu^{II} and Co^{III} η^1-superoxide intermediates, with the thermodynamics influenced by the destabilization of Co^{II} $TPQ_{sq\bullet+}$ relative to Cu^{I} $TPQ_{sq\bullet+}$. The semiquinone is detectable in anaerobic solutions of substrate-reduced CuA-

dx.doi.org/10.1021/jp3121484 | J. Phys. Chem. B XXXX, XXX, XXX−XXX

GAO but not CoAGAO, even when the enzyme is oxidized to Co^{III} before treatment with the primary amine.

Based on analysis of the kinetic parameters, reduction of the active site metal is at least 3 kcal mol^{-1} more favorable in Cu^{II} TPQ_{red} than in Co^{III} TPQ_{red}. Both reactions are required for O_2 coordination. The subsequent PCET is predicted to be 4−5 kcal mol^{-1} higher in energy for CuAGAO than CoAGAO based on DFT calculations. This result is consistent with the stabilization of the $Cu^{II}O_2^{-I}$ relative to the $Co^{III}O_2^{-I}$. The thermodynamics is therefore more favorable for the reaction of the higher energy $Co^{III}O_2^{-I}$ intermediate. The $\Delta\Delta G^{\ddagger}$ calculated for PCET (i.e., $\Delta G^{\ddagger}$ = 7.9 kcal mol^{-1} for CuAGAO versus $\Delta G^{\ddagger}$ = 3.0 kcal mol^{-1} for CoAGAO based on the DFT analysis) is in accord with the difference in $\Delta G^{\ddagger}$ of 4.5 kcal mol^{-1} estimated from the second order rate constants interpreted within the adiabatic limit.[84]

The DFT calculations have also predicted ^{18}O KIEs in good agreement with those observed for PCET reactions during catalysis by CuAGAO and CoAGAO. The derived transition states for O_2 reduction reveal similar Cu−O and Co−O interactions and the formation of O−H bonds of comparable strengths, which offset O−O bond weakening upon PCET. Evidence for such mechanisms is typically quite challenging to obtain. Yet, in this study, the combination of experiment and theory reveals that hydrogen bonding supports unidirectional proton-coupled electron transfer over a moderately large distance (~6 Å) between two redox cofactors. These findings further illustrate the potential of heavy atom kinetic isotope effects as mechanistic probes as well as their value as benchmarks for validating theoretical calculations.

■ ASSOCIATED CONTENT

Supporting Information

Kinetic, spectroscopic, and computational details, including vibrational frequencies and Cartesian coordinates. This material is available free of charge via the Internet at http://pubs.acs.org.

■ AUTHOR INFORMATION

Corresponding Author

*E-mail: jproth@jhu.edu.

Present Addresses

[‖]Department of Chemistry, University of Connecticut, 55 North Eagleville Road, Storrs, Connecticut 06269

[⊥]President's Office, University of Rhode Island, Campus Avenue, Kingston, Rhode Island 02881.

Notes

The authors declare no competing financial interest.

■ ACKNOWLEDGMENTS

Support for this work was provided by grants from the National Science Foundation (MCB0919898) and U.S. Department of Energy (DE-FG02-09ER16094) to J.P.R., the National Institutes of Health (GM27659) to D.M.D., and the Florida State Department of Health James and Esther King Biomedical Research Program (08KN-11) to R.P. We wish to thank Profs. Judith Klinman and Steve Mills for ongoing discussions.

■ REFERENCES

(1) Largeron, M.; Fleury, M.-B. *Angew.Chem., Int. Ed.* **2012**, *51*, 5409−5142.

(2) Piera, J.; Backvall, J.-E. *Angew.Chem., Int. Ed.* **2008**, *47*, 3506−3523.

(3) Punniyamurthy, T.; Velusamy, S.; Iqbal, J. *Chem. Rev.* **2005**, *105*, 2329−2963.

(4) Stahl, S. S. *Angew.Chem., Int. Ed.* **2004**, *43*, 3400−3420.

(5) Gamez, P.; Aubel, P. G.; Driessen, W. L.; Reedijk, J. *Chem. Soc. Rev.* **2001**, *30*, 376−385.

(6) Que, L., Jr; Tolman, W. B. *Nature* **2008**, *455*, 333−340.

(7) Solomon, E. I.; Chen, P.; Metz, M.; Lee, S.-K.; Palmer, A. E. *Angew.Chem., Int. Ed.* **2001**, *40*, 4570−4590.

(8) Mahadevan, V.; Gebbink, R. J. M. Klein; Stack, T. D. P. *Curr. Opin. Chem. Biol.* **2000**, *4*, 228−234.

(9) Klinman, J. P. *Chem. Rev.* **1996**, *96*, 2541−2562.

(10) Solomon, E. I.; Sundaram, U. M.; Machonkin, T. E. *Chem. Rev.* **1996**, *96*, 2563−2606.

(11) Roth, J. P. *Acc. Chem. Res.* **2009**, *42*, 399−408.

(12) Solomon, E. I.; Lowery, M. D. *Science* **1993**, *259*, 1575−1581.

(13) Siegbahn, P. E. M.; Borowski, T. *Acc. Chem. Res.* **2006**, *39*, 729−738.

(14) Cramer, C. J.; Tolman, W. B. *Acc. Chem. Res.* **2007**, *40*, 601−608.

(15) Siegbahn, P. E. M.; Blomberg, M. R. A. *Chem. Rev.* **2010**, *110*, 7040−7061.

(16) De La Lande, A.; Salahub, D. R.; Maddaluno, J.; Scemama, A.; Pilme, J.; Parisel, O.; Gerard, H.; Caffarel, M.; Piquemal, J.-P. *J. Comput. Chem.* **2011**, *32*, 1178−1182.

(17) Rokhsana, D.; Shepard, E. M.; Brown, D. E.; Dooley, D. M. In *Copper-Oxygen Chemsitry*; Karlin, K. D., Itoh S., Eds.; Wiley Series on Reactive Intermediates in Chemistry and Biology, 4 (Copper-Oxygen Chemistry); Wiley: New York, 2011; pp 53−106.

(18) Heuts, D. P.; Gummadova, J. O.; Pang, J.; Rigby, S. E.; Scrutton, N. S. *J. Biol. Chem.* **2011**, *286*, 29584−29593.

(19) Yu, P. H.; Wright, S.; Fan, E. H.; Lun, Z. R.; Gubisne-Harberle, D. *Biochim. Biophys. Acta* **2003**, *1647*, 193−199.

(20) Kishishita, S.; Okajima, T.; Kim, M.; Yamaguchi, H.; Hirota, S.; Suzuki, S.; Kuroda, S.; Tanizawa, K.; Mure, M. *J. Am .Chem. Soc* **2003**, *125*, 1041−1055.

(21) Juda, G. A.; Shepard, E. M.; Elmore, B. O.; Dooley, D. M. *Biochemistry* **2006**, *45*, 8788−8800.

(22) Shepard, E. M.; Okonski, K. M.; Dooley, D. M. *Biochemistry* **2008**, *47*, 13907−13920.

(23) Klinman, J. P. *Pro. Natl. Acad. Sci. U.S.A.* **2001**, *98*, 14766−14768.

(24) Janes, S. M.; Mu, D.; Wemmer, D.; Smith, A. J.; Kaur, S.; Maltby, D.; Burlingame, A. L.; Klinman, J. P. *Science* **1990**, *248*, 981−4.

(25) Mills, S. A.; Brown, D. E.; Dang, K.; Sommer, D.; Bitsimis, A.; Nguyen, J.; Dooley, D. M. *J. Biol. Inorg. Chem.* **2012**, *17*, 507−515.

(26) Smith, M. A.; Pirrat, P.; Pearson, A. R.; Kurtis, C. R. P.; Trinh, C. H.; Gaule, T. G.; Knowles, P. F.; Phillips, S. E. V.; McPherson, M. J. *Biochemistry* **2010**, *49*, 1268−1280.

(27) Okajima, T.; Kishishita, S.; Chiu, Y-C; Murakawa, T.; Kim, M.; Yamaguchi, H.; Hirota, S.; Kuroda, S.; Tanizawa, K. *Biochemistry* **2005**, *44*, 12041−12048.

(28) Mills, S. A.; Goto, Y.; Su, Q.; Plastino, J.; Klinman, J. P. *Biochemistry* **2002**, *41*, 10577−10584.

(29) Mills, S. A.; Klinman, J. P. *J. Am. Chem. Soc.* **2000**, *122*, 9897−9904.

(30) Padiglia, A.; Medda, R.; Pedersen, J. Z.; Agro, A. F.; Lorrai, A.; Murgia, B.; Floris, G. *J. Biol. Inorg. Chem.* **1999**, *4*, 608−613.

(31) Agostinelli, E.; De Matteis, G.; Mondovi, B.; Morpurgo, L. *Biochem. J.* **1998**, *330*, 383−387.

(32) Mure, M.; Mills, S. A.; Klinman, J. P. *Biochemistry* **2002**, *41*, 9269−9278.

(33) Shepard, E. M.; Dooley, D. M. *J. Biol. Inorg. Chem.* **2006**, *11*, 1039−1048.

(34) Dooley, D. M.; McGuirl, M. A.; Brown, D. E.; Turowski, P. N.; McIntire, W. S.; Knowles, P. F. *Nature* **1991**, *349*, 262−264.

(35) Turowski, P. N.; McGuirl, M. A.; Dooley, D. M. *J. Biol. Chem.* **1993**, *268*, 17680−17682.

(36) Roth, J. P. In *Copper-Oxygen Chemsitry*; Karlin, K. D., Itoh S., Eds.; Wiley: New York, 2011; Vol. 4 (Copper-Oxygen Chemistry),

Wiley series on Reactive Intermediates in Chemistry and Biology, pp 169−195.
(37) Roth, J. P. *Curr. Opin. Chem. Biol* **2007**, *11*, 142−150.
(38) Mukherjee, A.; Smirnov, V. V.; Lanci, M. P.; Brown, D. E.; Shepard, E. M.; Dooley, D. M.; Roth, J. P. *J. Am .Chem. Soc.* **2008**, *130*, 9459−9473.
(39) Humphreys, K. J.; Mirica, L. M.; Wang, Y.; Klinman, J. P. *J. Am. Chem. Soc.* **2009**, *131*, 4657−4663.
(40) Mirica, L. M.; McCusker, K. P.; Munos, J. W.; Liu, H. W.; Klinman, J. P. *J. Am. Chem. Soc.* **2008**, *130*, 8122−8123.
(41) Welford, R. W.; Lam, A.; Mirica, L. M.; Klinman, J. P. *Biochemistry* **2007**, *46*, 10817−10827.
(42) Mukherjee, A.; Brinkley, D. W.; Chang, K. M.; Roth, J. P. *Biochemistry* **2007**, *46*, 3975−3989.
(43) Roth, J. P.; Klinman, J. P. *Isotope Effects in Chemistry and Biology*; CRC Press: Boca Raton, FL, 2006; pp 645−669.
(44) Su, Q.; Klinman, J. P. *Biochemistry* **1998**, *37*, 12513−12525.
(45) Roth, J. P.; Wincek, R.; Nodet, G.; Edmondson, D. E.; McIntire, W. S.; Klinman, J. P. *J. Am. Chem. Soc.* **2004**, *126*, 15120−15131.
(46) Roth, J. P.; Klinman, J. P. *Pro. Natl. Acad. Sci. U.S.A.* **2003**, *100*, 62−67.
(47) Smirnov, V. V.; Roth, J. P. *J. Am. Chem. Soc.* **2006**, *128*, 16424−16425.
(48) Sarma, R.; Angeles-Boza, A. M.; Brinkley, D. W.; Roth, J. P. *J. Am. Chem. Soc.* **2012**, *134*, 15371−15386.
(49) Huff, G. S.; Doncheva, I. S.; Brinkley, D. W.; Angeles-Boza, A. M.; Mukherjee, A.; Cramer, C. J.; Roth, J. P. *Biochemistry* **2011**, *50*, 7375−7389.
(50) Roth, J. P.; Cramer, C. J. *J. Am. Chem. Soc.* **2008**, *130*, 7802−7803.
(51) Related approaches have been applied to assess various enzyme mechanisms (51−55): Saylor, B. T.; Reinhardt, L. A.; Lu, Z.; Shukla, M. S.; Nguyen, L.; Cleland, W. W.; Angerhofer, A.; Allen, K. N.; Richards, N. G. J. *Biochemistry* **2012**, *51*, 2911−2920.
(52) MacMillar, S.; Edmondson, D. E.; Matsson, O. *J. Am. Chem. Soc.* **2011**, *133*, 12319−12321.
(53) Wepukhulu, W. O.; Smiley, V. L.; Vemulapalli, B.; Smiley, J. A.; Phillips, L. M.; Lee, J. K. *Org. Biomolec. Chem.* **2008**, *6*, 4533−4541.
(54) Schramm, V. L. *J. Biol. Chem.* **2007**, *282*, 28297−28300.
(55) Ralph, E. C.; Hirschi, J. S.; Anderson, M. A.; Cleland, W. W.; Singleton, D. A.; Fitzpatrick, P. F. *Biochemistry* **2007**, *46*, 7655−7664.
(56) Lanci, M. P.; Smirnov, V. V.; Cramer, C. J.; Gauchenova, E. V.; Sundermeyer, J.; Roth, J. P. *J. Am. Chem. Soc.* **2007**, *129*, 14697−14709.
(57) Smirnov, V. V.; Lanci, M. P.; Roth, J. P. *J. Phys. Chem. A.* **2009**, *113*, 1934−1945.
(58) Ashley, D. C.; Brinkley, D. W.; Roth, J. P. *Inorg. Chem.* **2010**, *49*, 3661−3675.
(59) Popp, B. V.; Wendlandt, J. E.; Landis, C. R.; Stahl, S. S. *Angew.Chem., Int. Ed.* **2007**, *46*, 601−604.
(60) See the Supporting Information.
(61) Fielding, A. J.; Lipscomb, J. D.; Que, L. J. *J. Am. Chem. Soc.* **2012**, *134*, 796−799.
(62) Fielding, A. J.; Kovaleva, E. G.; Farquhar, E. R.; Lipscomb, J. D.; Que, L. J. *J. Biol. Inorg. Chem.* **2011**, *16*, 341−355.
(63) Bennett, B. *Curr. Top. Biophys.* **2002**, *26*, 49−57.
(64) Guy, R. D.; Fogel, M. L.; Berry, J. A. *Plant. Physiol* **1993**, *101*, 37−47.
(65) Hevel, J. M.; Mills, S. A.; Klinman, J. P. *Biochemistry* **1999**, *38*, 3683−3693.
(66) Frisch, M. J.; Trucks, G. W.; Schlegel, H. B.; Scuseria, G. E.; Robb, M. A.; Cheeseman, J. R.; Montgomery, J. A., Jr.; Vreven, T.; Kudin, K. N.; Burant, J. C.; Millam, J. M.; Iyengar, S. S.; Tomasi, J.; Barone, V.; Mennucci, B.; Cossi, M.; Scalmani, G.; Rega, N.; Petersson, G. A.; Nakatsuji, H.; Hada, M.; Ehara, M.; Toyota, K.; Fukuda, R.; Hasegawa, J.; Ishida, M.; Nakajima, T.; Honda, Y.; Kitao, O.; Nakai, H.; Klene, M.; Li, X.; Knox, J. E.; Hratchian, H. P.; Cross, J. B.; Bakken, V.; Adamo, C.; Jaramillo, J.; Gomperts, R.; Stratmann, R. E.; Yazyev, O.; Austin, A. J.; Cammi, R.; Pomelli, C.; Ochterski, J. W.; Ayala, P. Y.; Morokuma, K.; Voth, G. A.; Salvador, P.; Dannenberg, J. J.; Zakrzewski, V. G.; Dapprich, S.; Daniels, A. D.; Strain, M. C.; Farkas, O.; Malick, D. K.; Rabuck, A. D.; Raghavachari, K.; Foresman, J. B.; Ortiz, J. V.; Cui, Q.; Baboul, A. G.; Clifford, S.; Cioslowski, J.; Stefanov, B. B.; Liu, G.; Liashenko, A.; Piskorz, P.; Komaromi, I.; Martin, R. L.; Fox, D. J.; Keith, T.; Al-Laham, M. A.; Peng, C. Y.; Nanayakkara, A.; Challacombe, M.; Gill, P. M. W.; Johnson, B.; Chen, W.; Wong, M. W.; Gonzalez, C.; Pople, J. A. *Gaussian 03*; Gaussian, Inc.: Wallingford, CT, 2004.
(67) Perdew, J. P.; Yue, W. *Phys. Rev. B* **1986**, *33*, 8800−8802.
(68) Tripathi, G.; Clements, M. *J. Chem. Phys.* **2003**, *107*, 11125−11132.
(69) Tovrog, B. S.; Kitko, D. J.; Drago, R. S. *J. Am. Chem. Soc.* **1976**, *98*, 5144−5153.
(70) Mukherjee, A.; Angeles-Boza, A. M.; Huff, G. S.; Roth, J. P. *J. Am. Chem. Soc.* **2011**, *133*, 227−238.
(71) Danish, H. H.; Doncheva, I. S.; Roth, J. P. *J. Am. Chem. Soc.* **2011**, *133*, 15846−15849.
(72) Huynh, M. H.; Meyer, T. J. *Chem. Rev.* **2007**, *107*, 5004−5064.
(73) Dooley, D. M.; Scott, R. A.; Knowles, P. F.; Colangelo, C. M.; McGuirl, M. A.; Brown, D. E. *J. Am. Chem. Soc.* **1998**, *120*, 2599−2605.
(74) Medda, R.; Mura, A.; Longu, S.; Anedda, R.; Padiglia, A.; Casu, M.; Floris, G. *Biochimie* **2006**, *88*, 827−835.
(75) Medda, R.; Padiglia, A.; Bellelli, A.; Sarti, P.; Santanche, S.; Finazzi, A. A.; Floris, G. *Biochem. J.* **1998**, *332*, 431−437.
(76) Bellelli, A.; Agro, A. F.; Floris, G.; Brunori, M. *J. Biol. Chem.* **1991**, *266*, 20654−20657.
(77) Peterson, R. L.; Himes, R. A.; Kotani, H.; Suenobu, T.; Tian, L.; Siegler, M. A.; Solomon, E. I.; Fukuzumi, S.; Karlin, K. D. *J .Am .Chem. Soc.* **2011**, *133*, 1702−1705.
(78) Goto, Y.; Klinman, J. P. *Biochemistry* **2002**, *41*, 13637−13643.
(79) Prabhakar, R.; Siegbahn, P. E. M.; Minaev, B. F.; Ågren, H. . *J. Phys. Chem. B* **2004**, *108*, 13882−13892.
(80) Prabhakar, R.; Siegbahn, P. E.; Minaev, B. F. *Biochim. Biophys. Acta* **2003**, *1647*, 173−178.
(81) Lee, Y.; Sayre, L. M. *J. Am. Chem. Soc.* **1995**, *117*, 11823−11828.
(82) Wang, F.; Bae, J-Y; Jacobson, A. R.; Lee, Y.; Sayre, L. M. *J. Org. Chem.* **1994**, *59*, 2409−2417.
(83) Mure, M.; Klinman, J. P. *J. Am. Chem. Soc.* **1995**, *117*, 8698.
(84) Marcus, R. A.; Sutin, N. *Biochim. Biophys. Acta* **1985**, *811*, 265−322.